Condensed Antenna Structural Models for Dynamics Analysis

R. Levy
Ground Antenna and Facilities Engineering Section

Condensed degree-of-freedom (effective-mass) models are compared with large degree-of-freedom finite-element models of a representative antenna-tipping and alidade structure, for both "locked" and "free-rotor" configurations. It is shown that: a) the effective-mass models accurately reproduce the lower-mode natural frequencies of the finite element model; b) frequency responses for the two types of models are in agreement up to at least 16 rad/s for specific points; and c) transient responses computed for the same points are in good agreement. It is concluded that the effective-mass model, which best represents the five lower modes of the finite-element model, is a sufficient representation of the structure for future incorporation with a total servo control-structure dynamic simulation.

I. Introduction

The finite-element computer models of a typical large antenna-tipping structure and alidade comprise many more degrees of freedom, than can, or need be represented in a practical simulation of a combined structure and control-system dynamic response. Consequently, a drastic reduction of the structural finite-element model, to only a few equivalent degrees of freedom, is a necessary and a common practice. There are many known ways to achieve this reduction. Although differing in details of implementation, each of these ways are essentially equivalent in accurately representing only the low-frequency vibration modes and ignoring higher frequencies that are presumed to be outside of the operational control-system bandwidth.

The method of reduction used here is to represent each low-frequency vibration mode by an equivalent spring-mass single degree-of-freedom oscillator that is independent of the other modal oscillators. The formulation, which is given in Ref. 1, ensures that the reactions that result from independent rigid body acceleration of the structure foundation are the same for both the many degrees-of-freedom model and for the corresponding equivalent oscillators. This formulation is accomplished by matching the terms of the rigid-elastic modal coupling matrices of both the full structural model and the

equivalent oscillator model that represents the same modes. It can be shown that this condition also makes the kinetic energy of each oscillator equal to that of the corresponding structural mode for steady-state foundation motion. The inertia of higher-frequency modes, not represented by spring-mass oscillators, is contained in a residual mass placed at the foundation. Consequently, the mass of the full structure is accounted for; the approximation of this representation is only due to omitting the elasticity of the higher-frequency modes not represented by additional individual oscillators. It follows that the accuracy increases with larger numbers of effective oscillators. In the limit, a large set of oscillators provides a mathematically exact duplication of the dynamics of the original finite-element model.

This reduction method is chosen because of its accuracy, the simple representation it provides for the structure within a complete structure-servo control dynamics simulation program, and the ease of developing the effective oscillator properties. The equivalent oscillators are determined from special output provided by the JPL-IDEAS program eigenvalue analysis (Ref. 2). The output consists of a summary of the computations according to the algorithms of Ref. 1 for which principal relationships are restated and included here for reference in Appendix A. A restriction, that the equivalent representation applies only to systems that have statically determinate foundation reactions, is satisfied by the antenna structure.

II. Structure Models

The azimuth-axis drive control of an example 34-m diameter at the zenith position (elevation = 90°) will be considered. The elevation-axis drive model is similar with respect to representation of the tipping structure, but a separate treatment is necessary for the alidade representation. Figure 1 shows a representative tipping structure and alidade. The global Z-axis is the vertical axis. At zenith elevation, the reflector local Z (pointing) axis coincides with the global axis and at horizon elevation the local reflector Y-axis coincides with the global Z-axis.

The effective mass oscillators are derived from a JPL-IDEAS eigenvalue analysis of the finite-element model. The structure is foundation-grounded at the alidade base. Since we are concerned with the azimuth-axis drive, the only ground motion of interest is the alidade rotation about the Z-axis and the corresponding inertia term is the mass moment of inertia about this axis. Consequently, the effective "mass" model becomes an effective "mass moment of inertia" model with a torsional, rather than linear, spring constant. In the following discussions, references to "mass" and "inertia" will be used interchangeably to imply the "mass moment of inertia."

Figure 2(a) shows five effective mass oscillators that are established after screening the lowest 16 natural vibration modes found from the eigenvalue analysis. The screening eliminated modes with insignificant azimuth rotation and reduced the number of oscillators to the five that represent the first through the fourth and the thirteenth modes of the constrained model. These oscillators are combined with the residual inertia of the remaining unrepresented natural modes and with the azimuth gearbox springs. Motion of the alidade base (point B) is allowed, and Fig. 2(a) represents a "locked rotor" model grounded at the azimuth motor rotors. Figure 2(b) is the "free rotor" model with unconstrained azimuth rotors and with the reflected rotor inertia included at the two motor points (M1 and M2). Each motor point is associated with the azimuth drive consisting of the two motors and two gearboxes at each of the two corners of the alidade base. The control-system model transfer function for the effective-mass oscillators is described in Appendix B.

The conventional normal coordinates of the associated natural modes are related to the five effective oscillator coordinates by easily determined individual scale factors. These modal normal coordinates can be employed within the conventional method of modal analysis (Ref. 3) as "combining factors" that operate on the eigenvectors to synthesize the dynamic displacement response of the finite-element model by superposition. However, since the effective-mass coordinates are relative to the alidade base, the displacement of the base must be added to each displacement obtained from modal superposition.

III. Numerical Results

Table 1 provides the inertia and stiffness properties of the condensed models of Figs. 2(a) and 2(b). The five frequency numbers tabulated are from the eigenvalue analysis of the finite-element model grounded at the alidade base (no gear box springs) and are a subset of the first sixteen modes, as described previously. Notes in this table show how the residual inertia is determined for the azimuth base point of the model, and also show the calculations for reflected motor-rotor inertias and gearbox springs.

A. Natural Frequencies

Table 2 shows comparisons of the natural frequencies obtained from analysis of the models of Figs. 2(a) and 2(b), and the 12 lowest modes obtained from analysis of 3700 degree-of-freedom finite-element models that also contained the azimuth gearbox springs and the free rotor reflected motor inertias. There apparently is a spurious highest-mode frequency of the equivalent models, but otherwise the agreement with the full models ranges from excellent to good. The second mode

(4.9 rad/s) free-rotor natural frequency is not significant and represents a mode shape that consists essentially of the two motor rotors moving in opposition. This mode would be excited only in the case of a conflicting input command. Note that the lowest-mode frequency of the full model for the free-rotor case is almost, but not quite, equal to the ideal value of zero. This is because at the time of this investigation the IDEAS program did not accommodate a singular stiffness matrix except by the artifice of including an almost zero stiffness spring. More recently, however, a program update has been provided to treat the singular condition. Figure 3 shows a plot of the lowest 12 finite-element model natural frequencies to facilitate comparison of the "locked" and "free" rotor configurations. Where frequencies are almost the same for either configuration, it can be assumed that the mode does not entail significant rotation about the azimuth axis.

An additional NASTRAN program natural frequency analysis was made for the "free-rotor" finite-element model for comparison with the IDEAS "soft-spring" analysis. Table 3 shows the NASTRAN natural frequencies and repeats the values from Table 2 that were obtained with IDEAS. The frequencies compare well from the first through fifth modes and also for the seventh and eighth modes. The generalized masses computed for the eigenvectors of these same modes have also been found to be similar. There is no eigenvalue agreement after the eighth mode, and NASTRAN does not show several of the lower frequencies (which have been identified as local quadripod modes, found by IDEAS). Some differences between results of the two programs are expected because of small differences in the stiffness matrix formulation for membrane plate finite elements.

B. Steady-State Response

Forced steady-state frequency response calculations were made for the effective-mass models of Figs. 2(a) and 2(b) and also by conventional modal superposition analysis of the 12 lowest modes of complete finite-element models with gearbox springs and motor rotors. Damping was assumed to be negligible in these calculations. The natural frequencies of all of these models have been presented in Table 2.

The input to the "locked-rotor" models is a fixed amplitude, variable frequency sinusoidal torque applied at the alidade base. It can be shown that a similar dynamic response will occur when the torque excitation is replaced by prescribed equal sinusoidal displacements at the motor grounding points. Figure 4 shows the "locked-rotor" steady-state response for the alidade base ϕ_B, azimuth encoder ϕ_E, and alidade ϕ_A at forcing frequencies of up to 16 radians per second. The alidade response shown is defined as the rotation of the line between the elevation-bearing support points at the top of the alidade. Four sets of data are shown on each of the curves of Fig. 4: the full-model 12-mode response superposition computed by both the mode-displacement (M-D) and mode-acceleration (M-A) methods (Ref. 3); the response of the six degree-of-freedom (6 DOF) model of Fig. 2(a); and the response of a model (2 DOF) similar to that of Fig. 2(a), but with only one equivalent modal mass instead of five.

It can be seen that the full-model mode-acceleration method and the model of the responses of Fig. 2(a) are in agreement. These responses also are assumed to be the most accurate, based upon a check that can be made for zero forcing frequency. The mode-displacement and mode-acceleration methods' responses appear to converge at higher frequencies. The single effective-mass (2 DOF) model accuracy degenerates at frequencies above the 10.7 rad/s lowest-mode resonance. At forcing frequencies beyond the second mode resonance of 14.6 rad/s, this 2 DOF model is no longer valid.

The torque input to the "free-rotor" models is an equal pair applied at the two motors. The frequency response is shown in Figs. 7 through 10. Figures 7 through 9 show the responses for the same points as Figs. 4 through 6. Figure 10 shows the response curve for either one of the same motor points that were grounded for Figs. 4 through 6. The model 12-mode response is computed only by the mode-displacement method. As in Figs. 4 through 6, the response of the effective-mass model (8 DOF) is identical to the full-model response to within the scale of the figures. The response of a single effective-mass model (4 DOF) compares in accuracy to the response of the similar model (2 DOF) of Figs. 4 through 6. It is reassuring to observe that the motor response exhibits the conventional anti-resonances at the locked-rotor natural frequencies.

C. Transient Response

Transient responses of full structure and effective mass models are shown in Figs. 11 and 12. The rigid body motion of the free rotor models has been subtracted in Fig. 12. Time histories are shown for impulse-type forcing functions that consist of step torques of 0.02 seconds duration (instead of the sinusoidal functions used in the frequency response analysis in Figs. 4 through 10).

The solid lines in Figs. 11 and 12 are the responses for the effective-mass models determined by the Advanced Continuous Simulation Language (ACSL) program. The ACSL program was used to solve the differential equations for the models of Figs. 2(a) and 2(b) directly, although it could also use transfer function inputs. The broken lines represent the response superposition for the lowest 12 modes of the full finite-element model, which were obtained by an in-house program written for this purpose. In both "locked" and "free" rotor models, damping of 0.5% was applied for the lowest

significant elastic modes (10.7 and 11.3 rad/s) and the damping for the higher modes increased (damping matrices were proportional to stiffness matrices) in proportion to the natural frequency.

The above figures typically show essentially similar wave forms, although there are occasional differences in the amplitude peaks. These differences tend to be restricted to the initial half of the time histories. At the later times of the figures the full model and effective-mass model agreement improves. The differences in the earlier portion of the time histories is attributed to the presence of more higher-mode frequency content in the full model, which becomes attenuated later on by damping. Despite some differences in the transient response curve, the transient response agreement of the five effective modal-mass representations with the full model response is estimated to be adequate.

IV. Summary

The lower-mode natural frequencies have been shown to be identical in large finite-element models and condensed effective-mass models. Furthermore, the control-system bandpass cut-off frequency, usually less than about 2 rad/s, is within the range of frequencies for which the effective-mass models have shown good agreement with the full finite-element models for steady-state response. Consequently, the numerical results justify employing the effective-mass representation within the control-structure simulation model.

Acknowledgment

The author wishes to thank John Cucchissi for developing the computations and executing the computer models, and Douglas Strain who provided the software for the computer graphics.

References

1. Wada, B. K., Bamford, R., and Garba, J. A., "Equivalent Spring-Mass System: A Physical Interpretation," *The Shock and Vibration Bulletin*, No. 42, Part 5, pp. 215-225, January 1972.

2. Levy, R., "Optimization of Antenna Structure Design," *Eighth Conference on Electronic Computation*, ASCE, Houston, Texas, February 1983.

3. Bisplinghoff, R. L., Ashley, H., and Halfman, R. L., *Aeroelasticity*, Addison-Wesley Publishing Co., Reading, Massachusetts, Ch. 3, 1955.

Table 1. Equivalent-mass model data

Point	Mode* Simulated		Inertia in-lbf-s^2 $\times 10^{-7}$	Stiffness in-lbf/rad $\times 10^{-9}$
	No.	Rad/s		
1	1	13.59	3.686	6.808
2	2	15.71	0.186	0.429
3	3	15.26	1.486	3.458
4	4	15.90	0.725	1.831
5	13	35.53	3.652	46.090
	Sum		9.734(1)	
B	Alidade base frame		3.878(2)	
M1	One drive corner		51.200(3)	12.800(4)
M2	One drive corner		51.200(3)	12.800(4)

*In first 16 modes of finite-element model grounded at base frame.

Notes:

1. Total structure and parasitic inertia about azimuth axis = 1.3612×10^8 in-lbf/s^2.
2. Residual inertia of B = $1.3612 \times 10^8 - 9.734 \times 10^7$ = 3.878×10^7 in-lbf/sec^2.
3. Inertia of one motor armature and gearbox = 0.0907 lbf-ft-sec^2 at high speed = $0.0907 \times 12 \times (15.339)^2 = 2.56 \times 10^8$ in-lbf-sec^2 at 1 × speed = 5.12×10^8 in-lbf sec^2 for 2 motors.
4. Spring constant, one gearbox = 0.963×10^7 at pinion × (386.7" radius/15" wheel)^2 = 6.4×10^9 in-lbf/rad of 1 × speed = 12.8×10^9 in-lbf/rad for 2 boxes.

Table 2. Full and condensed model natural frequencies, rad/s

	Natural frequencies, rad/s			
	Locked Rotor		Free Rotor	
	Finite-element model (IDEAS)	Equivalent 6 DOF model (RESPONMAP)	Finite-element model (IDEAS)	Equivalent 8 DOF model (RESPONMAP)
1	10.70	10.71	0.17	0.00
2	14.64	14.65	4.89	4.99
3	15.10	15.21	11.28	11.28
4	15.74	15.74	14.67	14.67
5	19.00	22.05	15.10	15.21
6	19.10	55.12	15.75	15.74
7	21.70		21.88	22.23
8	23.05		23.05	55.15
9	25.54		25.53	
10	26.05		26.07	
11	26.37		26.31	
12	29.65		29.22	

Table 3. NASTRAN vs. IDEAS, finite-element model, free-rotor natural frequencies

NASTRAN model			IDEAS model		
Mode	Rad/s	General mass	Mode	Rad/s	General mass
1	0.00	2,592	1	0.11	2,589
2	4.88	11,393	2	4.89	11,380
3	11.32	103	3	11.28	103
4	14.89	272	4	14.67	119
5	15.51	129	5	15.10	113
6	20.39	23	6	15.75	22
7	21.99	124	7	21.88	114
8	23.68	715	8	23.05	651
			9	25.53	8
			10	26.07	6
			11	26.31	5
			12	29.22	84
9	33.79	69			
10	39.13	344			
11	40.89	51			
12	41.51	299			

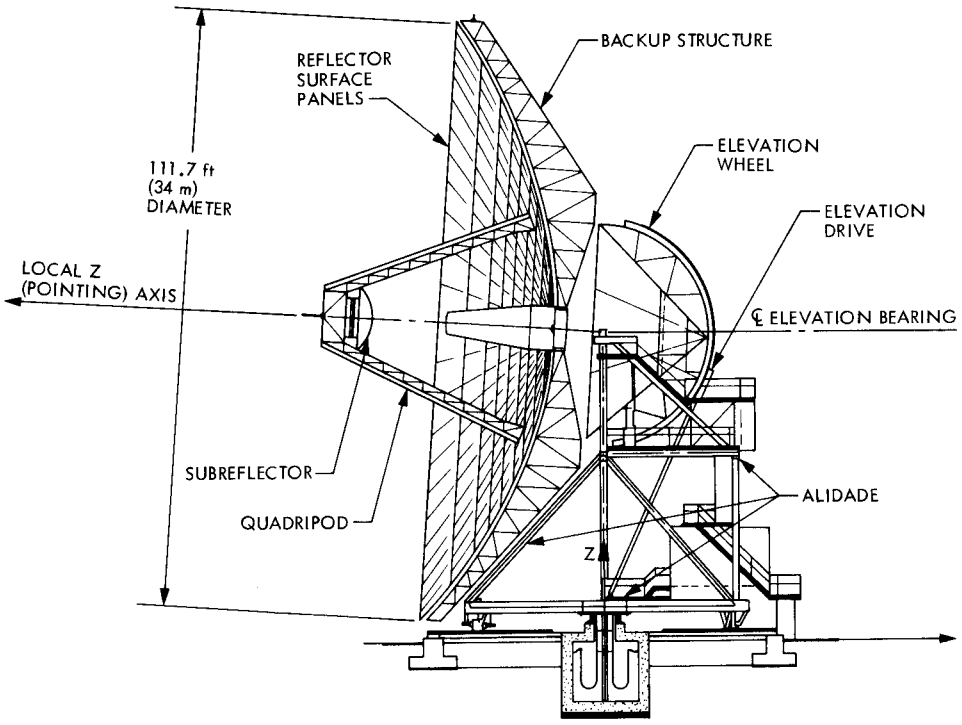

Fig. 1. Example antenna structure (34-m diameter)

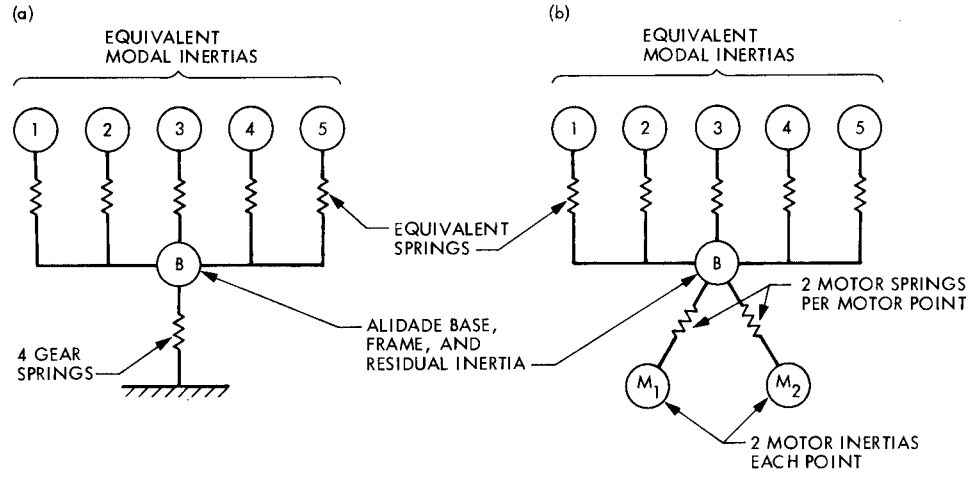

Fig. 2. Equivalent-mass models: (a) locked rotor; (b) free rotor

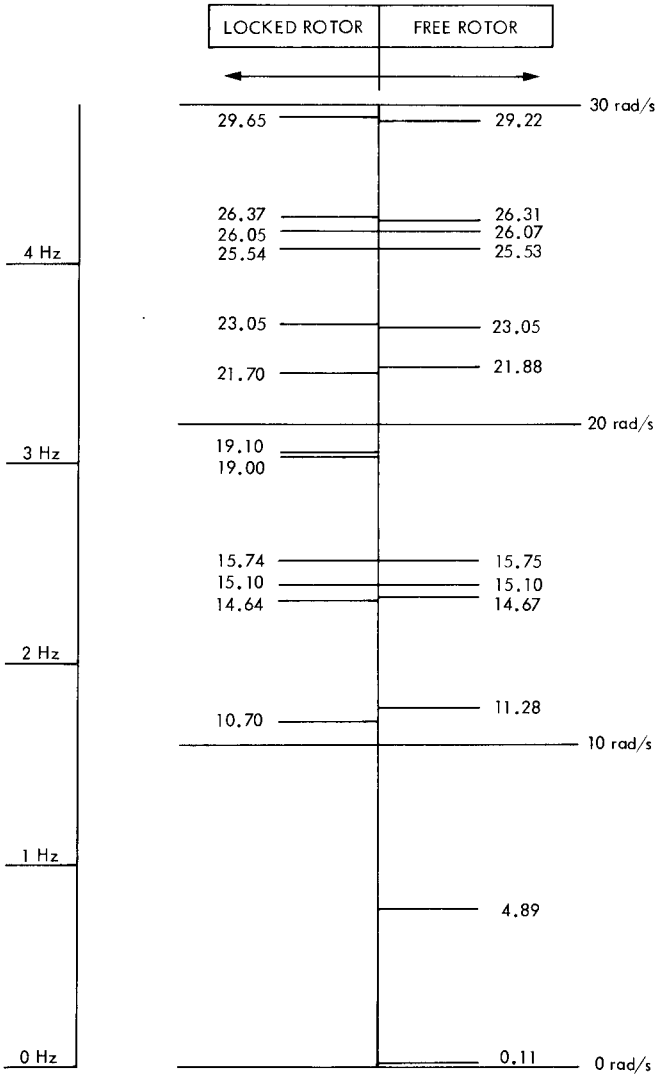

Fig. 3. Tipping and alidade structure natural frequencies, azimuth model (reflector at 90° elevation)

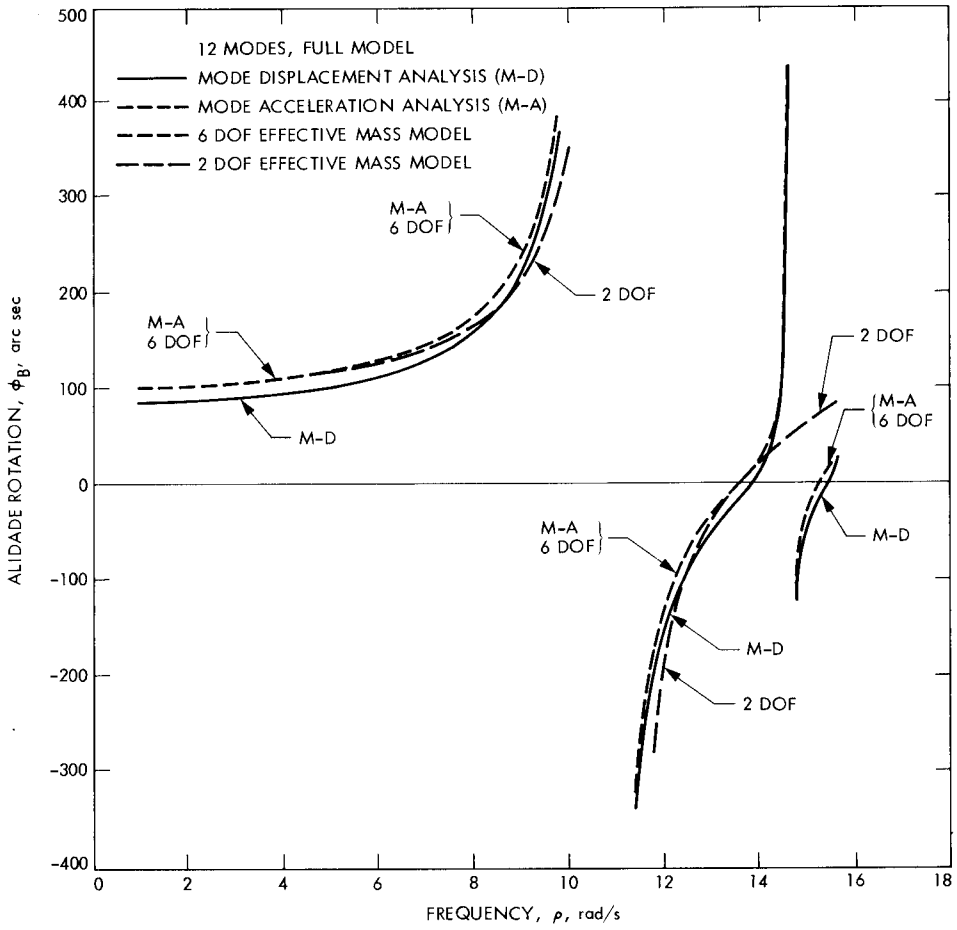

Fig. 4. Alidade base "locked-rotor" frequency response (K_s = 2.5518 x 10^{10} in-lbf/rad)

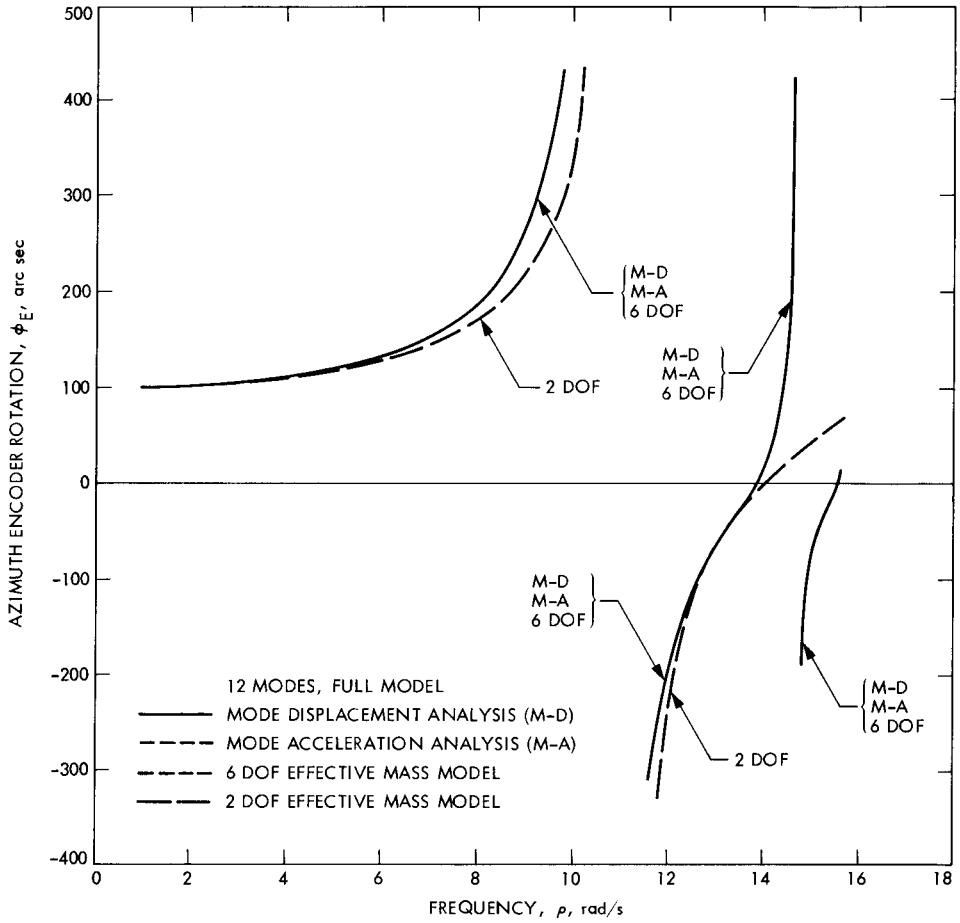

Fig. 5. Azimuth encoder "locked-rotor" frequency response (K_s = 2.5518 x 10^{10} in-lbf/rad)

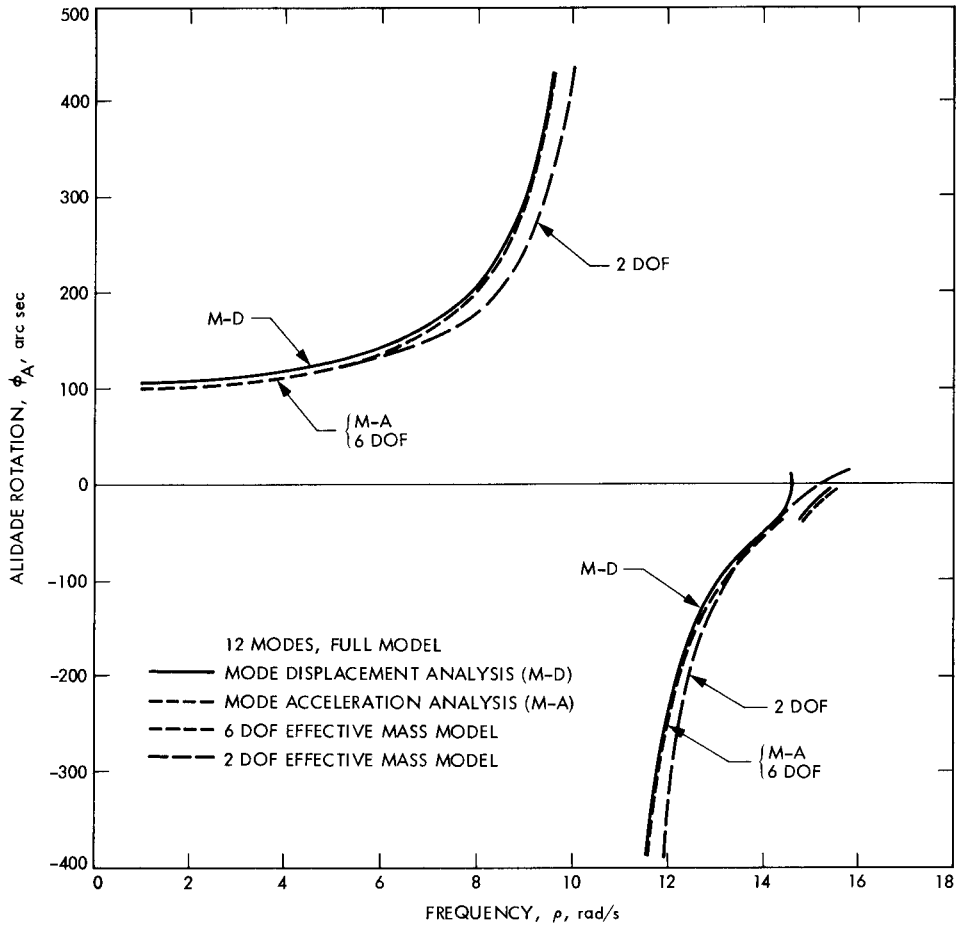

Fig. 6. Alidade "locked-rotor" frequency response (K_s = 2.5518 x 10^{10} in-lbf/rad)

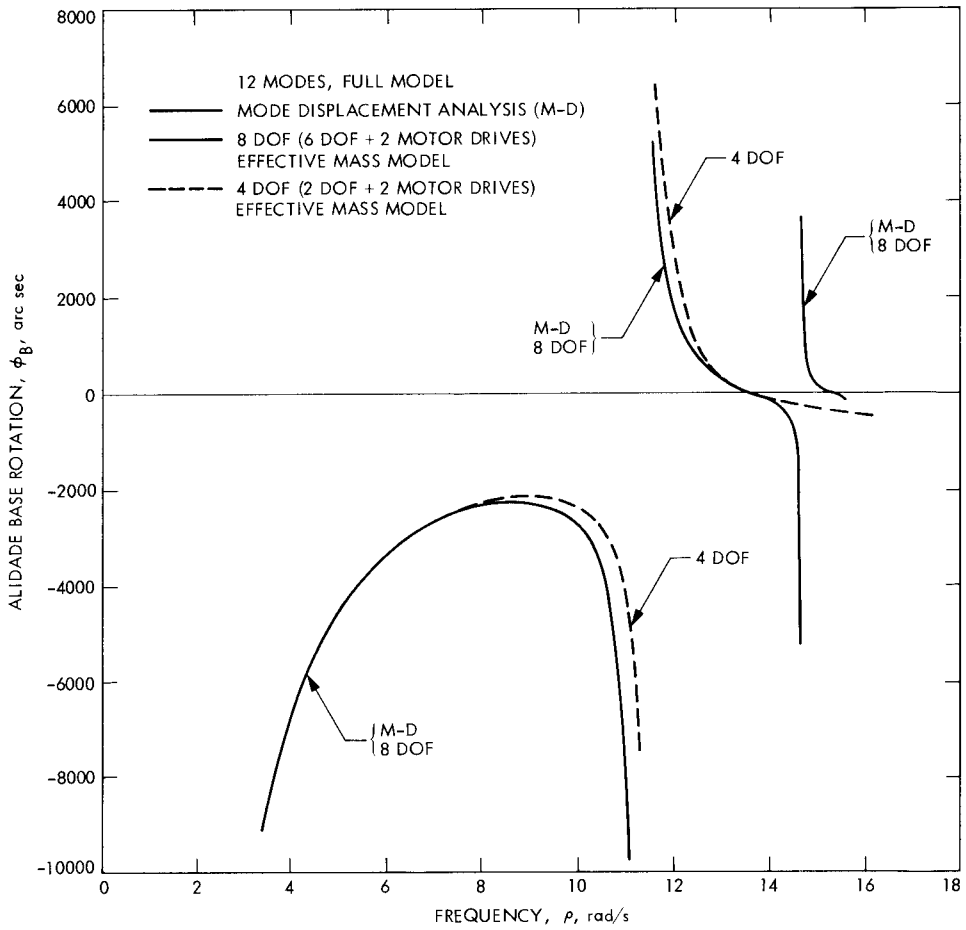

Fig. 7. Alidade base "free-rotor" frequency response (K_s = 2.5518 x 10^{10} in-lbf/rad)

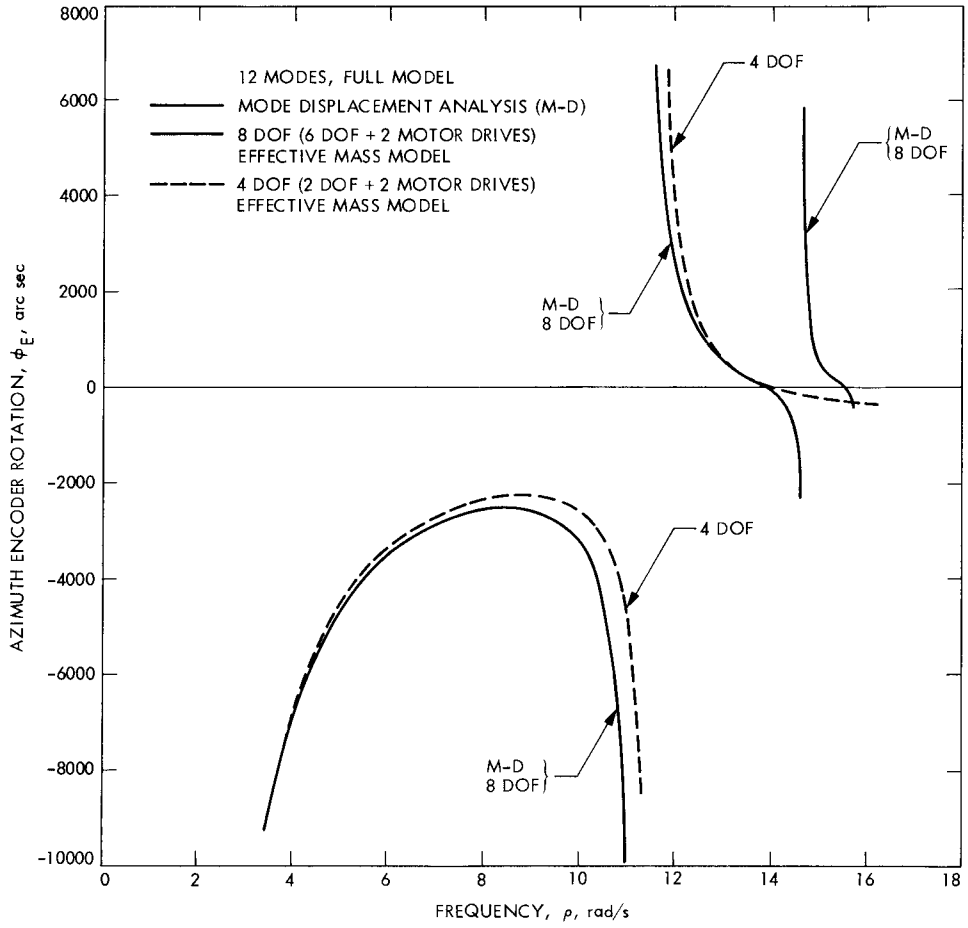

Fig. 8. Azimuth encoder "free-rotor" frequency response (K_s = 2.5518 x 10^{10} in-lbf/rad)

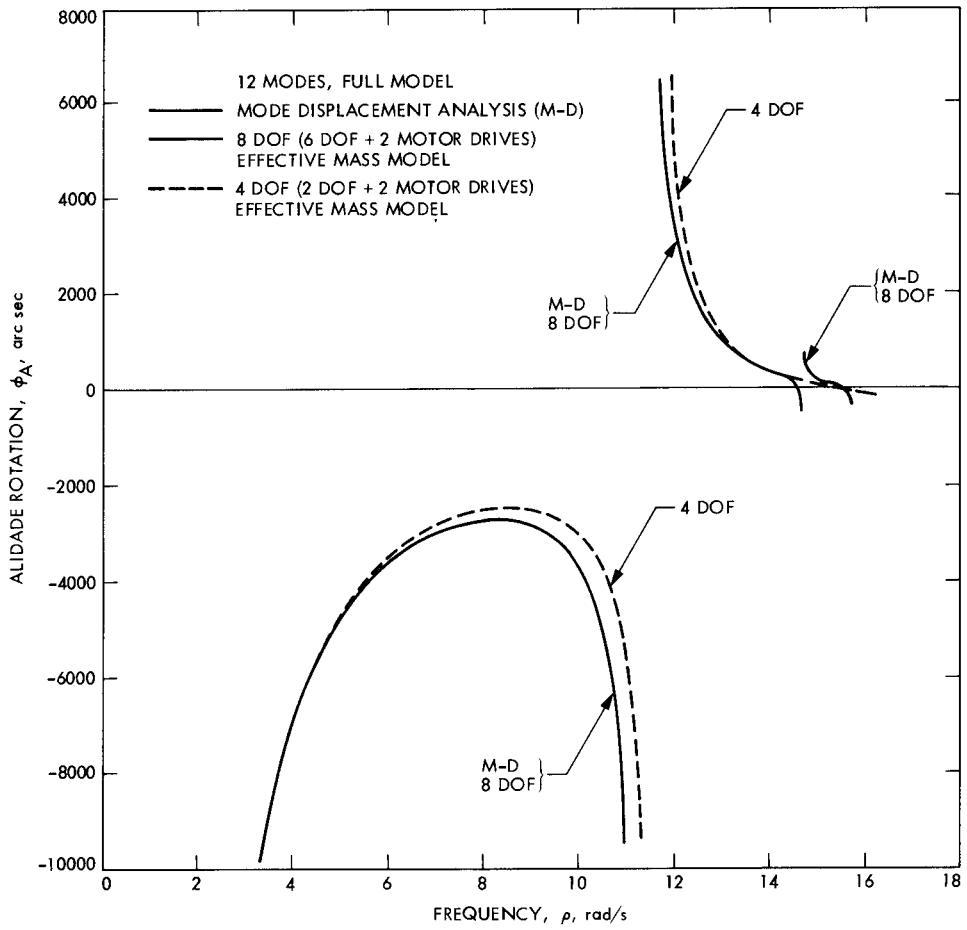

Fig. 9. Alidade "free-rotor" frequency response (K_s = 2.5518 x 10^{10} in-lbf/rad)

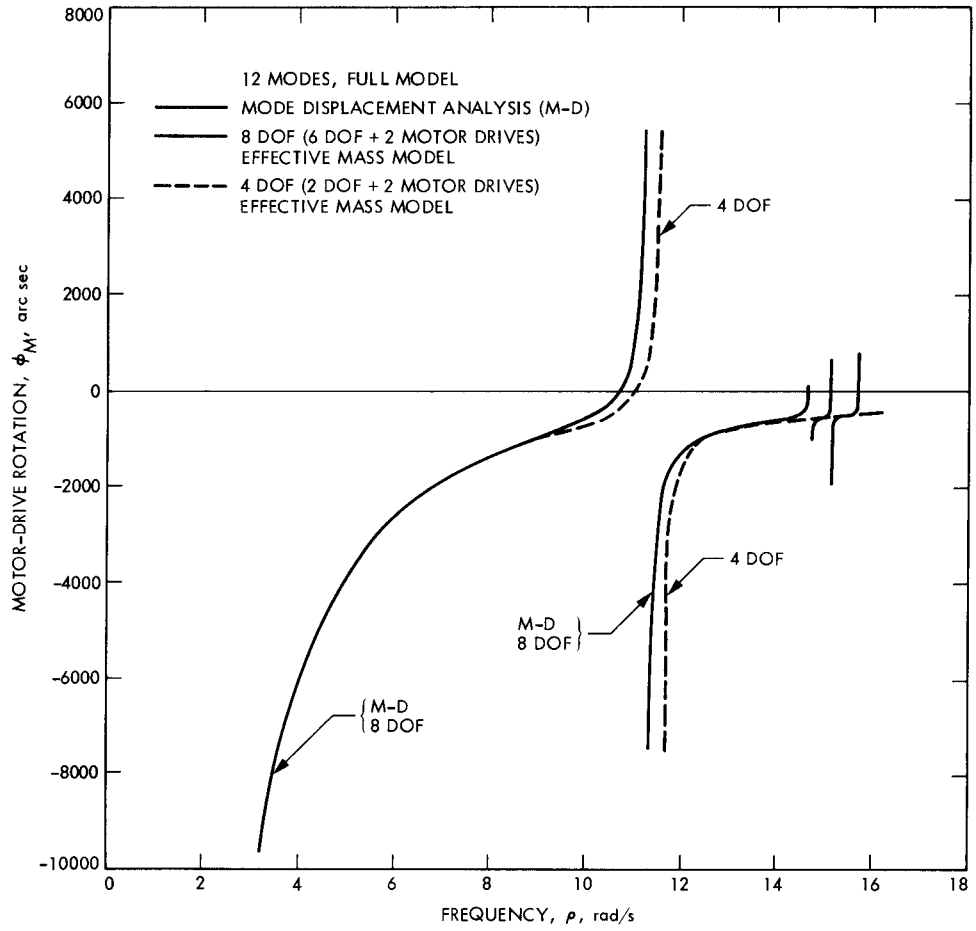

Fig. 10. Motor "free-rotor" frequency response (K_s = 2.5518 x 10^{10} in-lbf/rad)

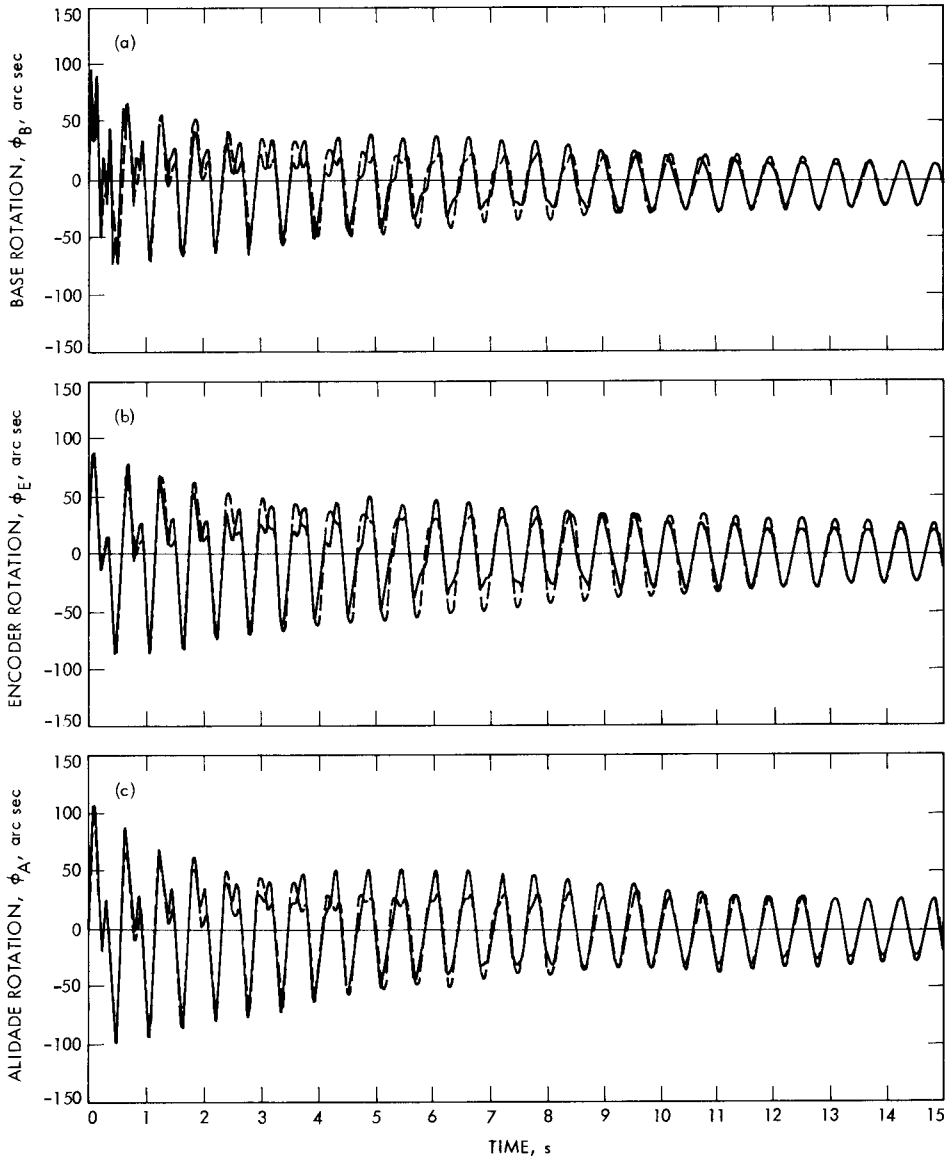

Fig. 11. ACSL versus modal-superposition, "locked rotor": (a) base; (b) encoder; (c) alidade

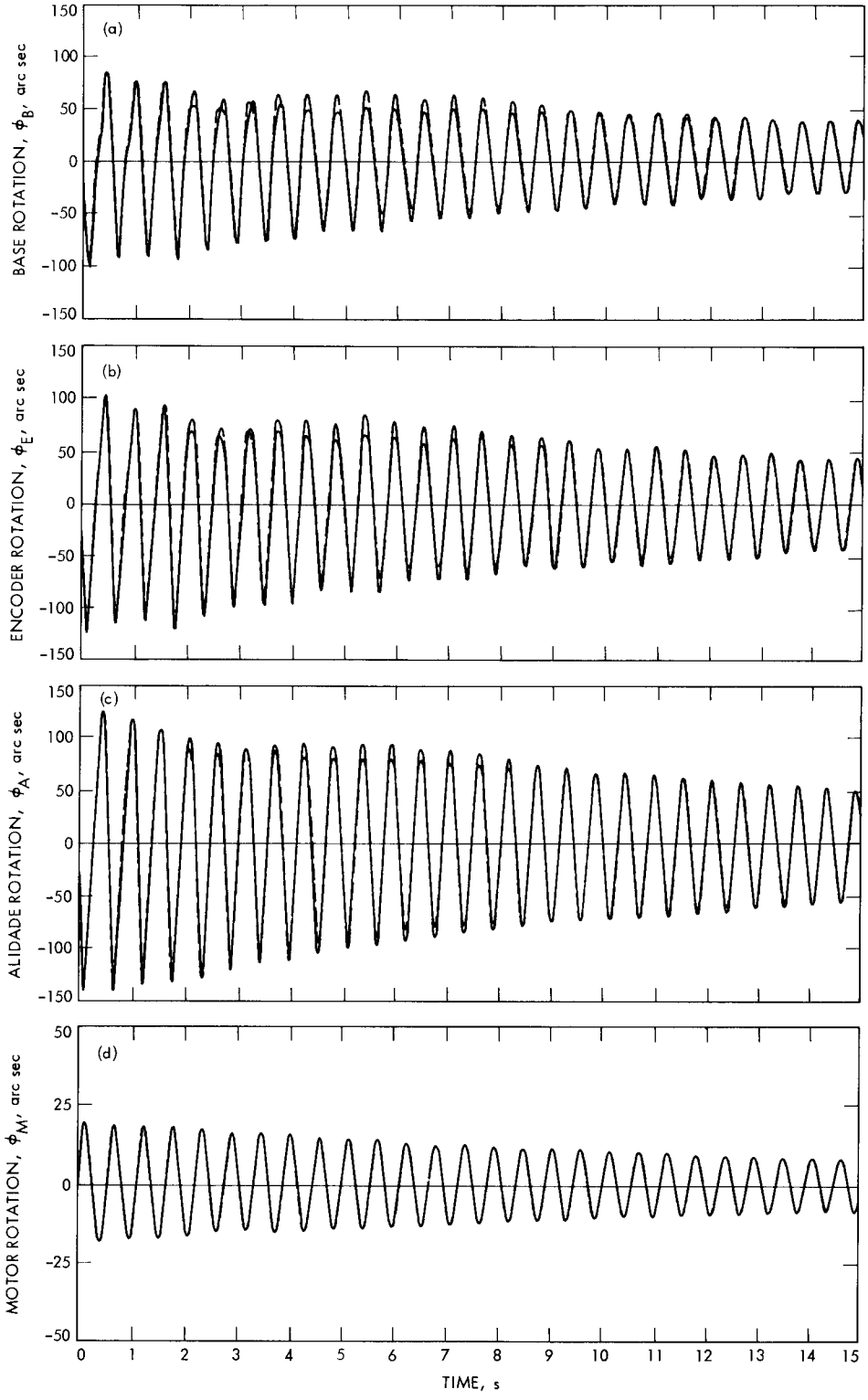

Fig. 12. ACSL versus modal-superposition, "free rotor": (a) base; (b) encoder; (c) alidade; (d) motor

Appendix A
Equivalent Oscillators Computations

The equations of motion of a linear, undamped elastic structure are:

$$\mathbf{M\ddot{u} + Ku = f} \tag{A-1}$$

$$\begin{Bmatrix} u \end{Bmatrix} = \begin{Bmatrix} x \\ g \end{Bmatrix} \tag{A-2}$$

in which

M = mass matrix

K = stiffness matrix

f = vector of forcing functions

u = set of all displacements

x = all displacements excluding the foundation

g = foundation displacements

When the structure has a statically determinate connection to the foundation, the displacements can be expressed as a combination of elastic and rigid body terms, e.g.

$$\mathbf{x = y + \phi_R g} \tag{A-3}$$

in which the foundation displacement has, at most, six components consisting of the three translations and three rotations that are listed in the following notation:

$$\mathbf{g} = [g_x\ g_y\ g_z\ g_{\theta x}\ g_{\theta y}\ g_{\theta z}]$$

and

y = set of elastic displacements

$\phi_{\mathbf{R}}$ = rigid body transformation; depends only on the geometry of nodes and the center of the foundation rotation

Each six rows of $\phi_{\mathbf{R}}$ correspond to the six degrees of freedom at each physical node of the structure model, and are of the form:

$$\text{typical rows of } \phi_{\mathbf{R}} = \begin{array}{c} \begin{matrix} (g_x) & (g_y) & (g_z) & (g_{\theta x}) & (g_{\theta y}) & (g_{\theta z}) \end{matrix} \\ \begin{bmatrix} 1 & 0 & 0 & 0 & Z' & -Y' \\ 0 & 1 & 0 & -Z' & 0 & X' \\ 0 & 0 & 1 & Y' & -X' & 0 \\ 0 & 0 & 0 & 1 & 0 & 0 \\ 0 & 0 & 0 & 0 & 1 & 0 \\ 0 & 0 & 0 & 0 & 0 & 1 \end{bmatrix} \end{array}$$

where X', Y', and Z' are the difference in the X, Y, and Z coordinates of the particular node and the center of the foundation rotation.

In the special case of a structure model that omits rotational degrees of freedom and contains only the three translations at each node, the last three rows of the above form are omitted. Beyond this, the remainder of the following development applies without other modifications.

For a structure with N nodes, we can write $\phi_{\mathbf{R}}$ as the following six column partitions

$$\phi_{\mathbf{R}} = [\{\phi_x\}\ \{\phi_y\}\ \{\phi_z\}\ \{\phi_{\theta x}\}\ \{\phi_{\theta y}\}\ \{\phi_{\theta z}\}] \tag{A-4}$$

where the form of each column repeats the six row (or three row, as explained) expression shown above.

Substituting Eq. (A-3) in Eq. (A-2), we have

$$\mathbf{u} = \begin{Bmatrix} \mathbf{x} \\ \mathbf{g} \end{Bmatrix} = \begin{bmatrix} \mathbf{I_{yy}} & \phi_{\mathbf{R}} \\ 0 & \mathbf{I_{gg}} \end{bmatrix} \begin{Bmatrix} \mathbf{y} \\ \mathbf{g} \end{Bmatrix} \tag{A-5}$$

in which $\mathbf{I_{yy}}$ and $\mathbf{I_{gg}}$ are identity matrices of the size of **y** and of **g**.

From conventional synthesis of normal modes, the elastic displacements are

$$\mathbf{y} = \phi_{\mathbf{N}}\xi \tag{A-6}$$

in which

$\phi_{\mathbf{N}}$ = matrix of eigenvectors ("modal matrix")

ξ = vector of "normal" modal coordinates

By substituting Eq. (A-5) in Eq. (A-6), we have

$$\mathbf{u} = \begin{Bmatrix} \mathbf{x} \\ \mathbf{g} \end{Bmatrix} = \begin{bmatrix} \phi_N & \phi_R \\ 0 & \mathbf{I}_{gg} \end{bmatrix} \begin{Bmatrix} \xi \\ \mathbf{g} \end{Bmatrix} \tag{A-7}$$

By partitioning Eq. (A-1) to conform with Eq. (A-7), making that substitution, and considering only the mass matrix $\mathbf{M}_{yy}$ associated with the elastic displacements, we have

$$\begin{bmatrix} \mathbf{M}_{yy} & 0 \\ 0 & 0 \end{bmatrix} \begin{bmatrix} \phi_N & \phi_R \\ \mathbf{u} & \mathbf{I}_{gg} \end{bmatrix} \begin{Bmatrix} \ddot{\xi} \\ \ddot{\mathbf{g}} \end{Bmatrix} + \begin{bmatrix} \mathbf{K}_{yy} & \mathbf{K}_{yg} \\ \mathbf{K}_{gy} & \mathbf{K}_{gg} \end{bmatrix} \begin{bmatrix} \phi_N & \phi_R \\ 0 & \mathbf{I}_{gg} \end{bmatrix} \begin{Bmatrix} \xi \\ \mathbf{g} \end{Bmatrix} = \begin{Bmatrix} \mathbf{f}_y \\ \mathbf{f}_g \end{Bmatrix} \tag{A-8}$$

where K_{yy}, K_{yg}, K_{gy}, K_{gg}, f_y, and f_g are the conforming partitions of the mass matrix and of the forcing function.

Equation (A-8) is premultiplied by the transpose

$$\begin{bmatrix} \phi_N & \phi_R \\ 0 & \mathbf{I}_{gg} \end{bmatrix}^t = \begin{bmatrix} \phi_N^t & 0 \\ \phi_R^t & \mathbf{I}_{gg} \end{bmatrix} \tag{A-9}$$

with the result

$$\left[\begin{array}{ccc|ccc} \phi_N^t & \mathbf{M}_{yy} & \phi_N & \phi_N^t & \mathbf{M}_{yy} & \phi_R \\ \hline \phi_R^t & \mathbf{M}_{yy} & \phi_N & \phi_R^t & \mathbf{M}_{yy} & \phi_R \end{array}\right] \begin{Bmatrix} \ddot{\xi} \\ \ddot{\mathbf{g}} \end{Bmatrix}$$

$$+ \left[\begin{array}{ccc|ccc} \phi_N^t & \mathbf{K}_{yy} & \phi_N & \phi_N^t & \mathbf{K}_{yy} & \phi_R + \phi_N^t \mathbf{K}_{yg} \\ \hline \phi_R^t & \mathbf{K}_{yy} & \phi_N & \phi_R^t & \mathbf{K}_{yy} & \phi_R + \phi_R^t \mathbf{K}_{yg} \\ + & \mathbf{K}_{gy} & \phi_N & + & \mathbf{K}_{gg} & + \mathbf{K}_{gy} \phi_R \end{array}\right] \begin{Bmatrix} \ddot{\xi} \\ \ddot{\mathbf{g}} \end{Bmatrix}$$

$$= \left\{\begin{array}{ccc} \phi_N^t & & \mathbf{f}_y \\ \hline \phi_R^t & \mathbf{f}_y & + \mathbf{f}_g \end{array}\right\} \tag{A-10}$$

The second coefficient matrix on the left-hand side of Eq. (A-10) can be significantly simplified. The simplification is obtained by considering only cases of rigid body displacements of the structure and foundation. In this case, all elastic displacements and displacement derivatives are zero, and only the foundation displacements can be non-zero. Then it can be concluded, from the principle that forces and reactions are zero for rigid body displacements, that only the upper-left partition of this matrix is not null. Therefore, we can rewrite Eq. (A-10) as

$$\begin{bmatrix} \mathbf{M}_{NN} & \mathbf{M}_{ER} \\ \mathbf{M}_{RE} & \mathbf{M}_{RR} \end{bmatrix} \begin{Bmatrix} \ddot{\xi} \\ \ddot{\mathbf{g}} \end{Bmatrix} + \begin{bmatrix} \mathbf{K}_{NN} & 0 \\ 0 & 0 \end{bmatrix} \begin{Bmatrix} \xi \\ \mathbf{g} \end{Bmatrix} = \begin{Bmatrix} \phi_N^t & \mathbf{f}_y \\ \phi_R^t \mathbf{f}_y & + \mathbf{f}_g \end{Bmatrix} \tag{A-11}$$

in which

$\mathbf{M}_{NN} = \phi_N^t \mathbf{M}_{yy} \phi_N$, the elastic-structure generalized mass matrix

$\mathbf{M}_{ER} = \phi_N^t \mathbf{M}_{yy} \phi_R$, the elastic-rigid coupling matrix

$\mathbf{M}_{RE} = \mathbf{M}_{ER}^t$, the rigid-elastic coupling matrix

$\mathbf{M}_{RR} = \phi_R^t \mathbf{M}_{yy} \phi_R$, the rigid-body mass matrix

$\mathbf{K}_{NN} = \phi_N^t \mathbf{K}_{yy} \phi_N$, the elastic-structure generalized stiffness matrix

Note from the orthogonality of the normal modes, that $\mathbf{M}_{NN}$ and $\mathbf{K}_{NN}$ are diagonal.

Equation (A-11), except for differences in notation and ordering, is identical to Eq. (A-4) of the reference.

When a full set of the maximum of six independent foundation displacements is considered, the elastic-rigid coupling matrix $\mathbf{M}_{ER}$ has one row for each normal mode included and one column for each of the six foundation displacements. A specific row of $\mathbf{M}_{ER}$ corresponding to the j^{th} normal mode can be written as

$$M_{ERj} = \begin{bmatrix} M_j^x & M_j^y & M_j^z & M_j^{\theta x} & M_j^{\theta y} & M_j^{\theta z} \end{bmatrix} \tag{A-12}$$

in which, for example

$$M_j^x = \phi_{Nj}^t \mathbf{M}_{yy} \phi_x$$

where ϕ_{Nj} is the j^{th} natural mode eigenvector and ϕ_x is the first column of the column-partitioned form of ϕ_R, as described following Eq. (A-3) and in Eq. (A-4). The remaining righthand-side terms are computed similarly by substituting the corresponding column of ϕ_R. Furthermore, the generalized mass of the j^{th} normal mode follows from the definition of the $\mathbf{M}_{NN}$ matrix Eq. (A-11) as

$$M_{NNj} = \phi_{Nj}^t \mathbf{M}_{yy} \phi_{Nj} \tag{A-13}$$

The notation of Eqs. (A-12) and (A-13) allows, as an example, the following term to be defined:

$$M_{Exj} = \left(M_j^x\right)^2 / M_{NNj}\, Sgn\left(M_j^x\right) \qquad \text{(A-14)}$$

Obviously, five more terms (M_{Eyj}, M_{Ezj}, $M_{E\theta xj}$, $M_{E\theta yj}$, and $M_{E\theta zj}$), similar in form to Eq. (A-14), can be generated by employing the second through sixth right-hand terms of Eq. (A-12) to replace, in turn, the $\mathbf{M}_j^x$ term of Eq. (A-14). Algebraic manipulations can show that forming the sum of the absolute values of the first three terms generated this way provides the j^{th} mode equivalent (effective) mass as defined in the reference. That is,

$$M_{Ej} = abs\,(M_{Exj}) + abs\,(M_{Eyj}) + abs\,(M_{Ezj}) \qquad \text{(A-15)}$$

It can also be shown that the six terms, M_{Exj} through $M_{E\theta zj}$, are the reductions to the diagonals of the residual mass matrix $\mathbf{M_{RES}}$ produced by the j^{th} normal mode. As a specific example, the k^{th} diagonal term of the residual mass matrix when **M** normal modes are included is given by

$$\mathbf{M_{RES}}\,(k, k) = \mathbf{M_{RR}}\,(k, k) - \sum_{j=1}^{M} abs\,(M_{Epj}) \qquad \text{(A-16)}$$

where $p = x, y, z, \theta x, \theta y$, and θz for $k = 1, 2, 3, 4, 5$, and 6, respectively.

Evidently, if all natural modes are considered, the residual mass matrix will be zero. Also, if a diagonal term of $\mathbf{M_{RES}}$ is relatively large in comparison with the same diagonal of $\mathbf{M_{RR}}$, most of the inertia is being treated as rigid, and very little of it is being recognized as flexible. Nevertheless, such a representation could be appropriate if the **M** modes included adequately cover the spectrum of the structure frequencies that could be excited by the control system. Furthermore, if no normal (elastic) modes are considered, the following equality holds:

$$\mathbf{M_{RES}} = \mathbf{M_{RR}} \qquad \text{(A-17)}$$

When the mechanical control-system model is for an azimuth-elevation antenna, we are concerned with, at most, two rotational components of the foundation displacement vector. As a specific example, say we are concerned only with the azimuth-drive axis, which is identified here as the Z-axis. Then, the pertinent foundation displacement is $g_{\theta x}$. The significant terms of the rigid body and residual mass matrices are $\mathbf{M_{RR}}$ (6,6) and $\mathbf{M_{RES}}$ (6,6). Of the six terms that can be generated on the form of Eq. (A-14), only the last term $M_{E\theta zj}$ is needed. This latter term becomes the j^{th} mode equivalent inertia which is employed instead of the equivalent mass of Eq. (A-15).

The JPL-IDEAS computer program eigenvalue analysis performs the following related operations:

(1) Computes eigenvalues, eigenvectors, and generalized mass for the **M** user denoted lowest-frequency natural modes.

(2) Computes the six components of $\mathbf{M_{ER}}$ (see Eq. A-14) for each of the modes.

(3) Computes and tabulates the six reduction components to the diagonals of the residual mass matrix (see Eq. A-14) and equivalent mass (see Eq. A-15) for each mode.

(4) Computes and prints the 6 x 6 rigid-body mass matrix $\mathbf{M_{RR}}$ (see Eq. A-11).

(5) Computes and prints coordinates to locate the equivalent effective mass of each mode. The computations are not described here, but are consistent with formulations shown in the reference paper.

(6) Lists the sum of reductions to each of the diagonals of the residual mass matrix and the diagonals of the residual mass matrix for the **M** modes.

Appendix B

Transfer Function of Equivalent Modal Inertia Structure Model

A complex elastic structure can be simply represented within a mechanical control-system simulation model by the "candelabra" diagram of Fig. B-1. Here the parallel branches represent equivalent effective oscillators derived from the normal modes of the structure, and the stem represents physical coordinates of the output pinion of the gearbox that drives the system and of the motor that applies driving torques through the gearbox. The remainder of the control system, which interfaces with the motor and pinion, does not permit such simple generalization and is omitted from the figure.

The following notations are used in conjunction with Fig. B-1:

$q_1, \cdots, q_M$ = generalized elastic-effective modal coordinates derived from the "locked-rotor" (fixed at pinion) natural modes of the structure

$J_1, \cdots, J_M$ = equivalent inertia of the effective coordinates

$K_1, \cdots, K_M$ = equivalent stiffness of the effective coordinates

ω_{ni} = i^{th} mode structure natural circular frequency $(K_i/J_i)^{1/2}$

θ_P = gearbox pinion coordinate

J_P = gearbox inertia (includes residual inertia of structure, which is the inertia not included in J_1 through J_M)

K_G = gearbox spring constant

θ_{MTR} = coordinate of motor (input end of gearbox)

J_{MTR} = motor inertia

The typical equation of motion for the i^{th} modal oscillator is

$$J_i q_i + K_i (q_i - \theta_P) = 0, \quad i = 1, 2, \cdots, M \tag{B-1}$$

The pinion equation of motion is

$$J_P \ddot{\theta}_P + \sum_{i=1}^{M} K_i (\theta_P - q_i) + \sum_{j=1}^{L} K_G \left(\theta_P - \theta_{MTR_j}\right) = 0 \tag{B-2}$$

in which it has been assumed that there are L motors (with generic index, j) and gearboxes all attached to the same pinion.

The motor equation of motion is of the form

$$J_{MTR_j} \ddot{\theta}_{MTR_j} + K_G \left(\theta_{MTR_j} - \theta_P\right) + \text{Control System Terms} = \text{Motor Input Torque} \tag{B-3}$$

In Eqs. (B-1), (B-2), and (B-3) we have assumed an undamped structure and gearbox ratios of unity. These are not essential assumptions and are made here only to condense the discussions.

It is convenient to recast the equations of motion into relative oscillator coordinates. To do this, let e_i be the coordinate for the i^{th} oscillator relative to its base θ_P. That is

$$e_i = q_i - \theta_P$$

or (B-4)

$$q_i = e_i + \theta_P$$

Then Eq. (B-1) becomes

$$J_i \ddot{e}_i + K_i e_i = -J_i \ddot{\theta}_P, \quad i = 1, 2, \cdots, M \tag{B-5}$$

Using the Laplace operator S, the associated transfer functions become

$$e_i(S) = \frac{-S^2}{S^2 + \omega_{ni}^2} \theta_P(S) \tag{B-6}$$

Equation (B-2) can be written as

$$J_P \ddot{\theta}_P - \sum_{i=1}^{M} K_i e_i + \sum_{j=1}^{L} K_G \left(\theta_P - \theta_{MTR_j}\right) = F_P$$

or (B-7)

$$J_P \ddot{\theta}_P = \sum_{i=1}^{M} K_i e_i + \sum_{j=1}^{L} K_G \theta_{MTR_j} - \sum K_G \theta_P$$

so that the transfer function becomes

$$\theta_P(S) = \frac{\sum_{i=1}^{M} K_i e_i(S) + \sum_{j=1}^{L} K_G \theta_{MTR_j}(S) - \sum K_G \theta_P(S)}{J_P S^2} \tag{B-8}$$

The inertia, spring constant, and natural frequency of each e_i is the effective value associated with the i^{th} normal mode. If ξ_i is the normal coordinate of the i^{th} mode, it can be shown

$$\xi_i = \alpha_i e_i \tag{B-9}$$

where

$$\alpha_i = \sqrt{\frac{J_i}{JG_i}}$$

and JG_i is the generalized mass of the i^{th} mode, arbitrarily normalized according to the normalization of the eigenvector. Then let ϕ_{Ei} equal the value of the eigenvector of the encoder in the i^{th} mode, and θ_E equal the encoder displacement (in physical coordinates). It then follows from conventional modal analysis and the conversion here to relative coordinates that

$$\theta_E = \sum_{i=1}^{M} \phi_{Ei} \xi_i + \theta_P \tag{B-10}$$

By introducing the new constants

$$A_{Ei} = \phi_{Ei} \alpha_i \tag{B-11}$$

we have, from Eqs. (B-9), (B-10), and (B-11),

$$\theta_E = \sum_{i=1}^{M} A_{Ei} e_i + \theta_P \tag{B-12}$$

A servo-block diagram equivalent to Fig. B-1 is shown in Fig. B-2. This figure incorporates the relationships of Eqs. (B-6), (B-8), and (B-12), a non-unity gear ratio N, and four independent drive motors.

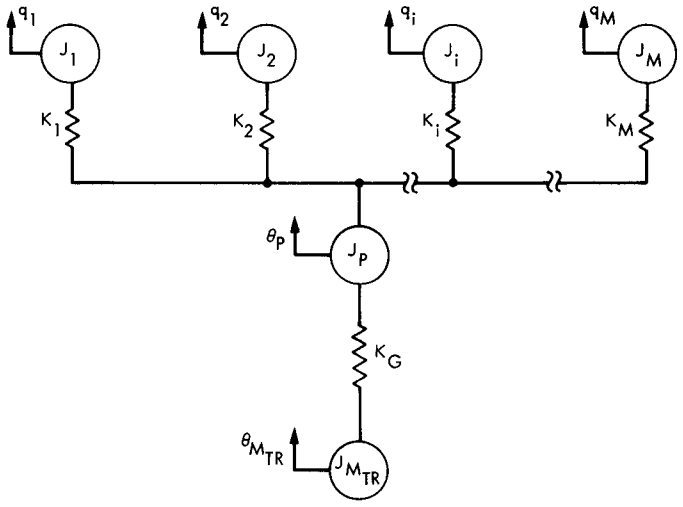

Fig. B-1. Structure model with equivalent modal oscillators

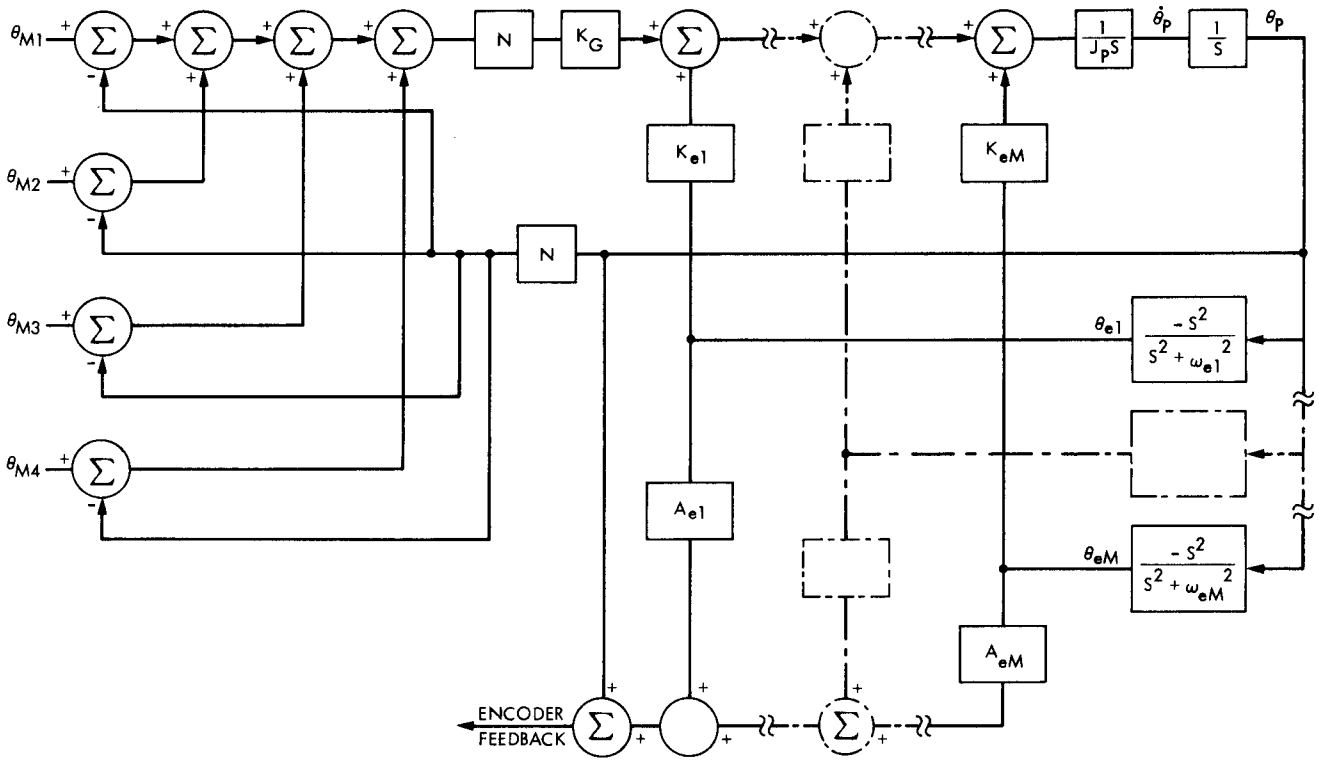

Fig. B-2. Servo-block diagram: equivalent modal inertia transfer functions within motor gearbox drive system